



Time-clustering behavior of spreading-center seismicity between 15 and 35°N on the Mid-Atlantic Ridge: observations from hydroacoustic monitoring

DelWayne R. Bohnenstiehl^{a,*}, Maya Tolstoy^a, Deborah K. Smith^b,
Christopher G. Fox^c, Robert P. Dziak^d

^a Lamont-Doherty Earth Observatory of Columbia University, 61 Route 9W, Palisades, NY 10964, USA

^b Woods Hole Oceanographic Institution, Woods Hole, MA 02549, USA

^c National Oceanic and Atmospheric Administration, Pacific Marine Environmental Laboratory,
Hatfield Marine Science Center, Newport, OR 97365, USA

^d Cooperative Institute for Marine Resource Studies, Oregon State University, Hatfield Marine Science Center, Newport, OR 97365, USA

Received 18 October 2002; accepted 22 April 2003

Abstract

An earthquake catalog derived from the detection of seismically-generated T-waves is used to study the time-clustering behavior of moderate-size (≥ 3.0 M) earthquakes between 15 and 35°N along the Mid-Atlantic Ridge (MAR). Within this region, the distribution of inter-event times is consistent with a non-periodic, non-random, clustered process. The highest degrees of clustering are associated temporally with large mainshock-aftershock sequences; however, some swarm-like activity also is evident. Temporal fluctuations characterized by a power spectral density $P(f)$ that decays as $1/f^\alpha$ are present within the time sequence, with α ranging from 0.12 to 0.55 for different regions of the spreading axis. This behavior is negligible at time scales less than $\sim 5 \times 10^3$ s, and earthquake occurrence becomes less clustered (smaller α) as increasing size thresholds are applied to the catalog. A power-law size-frequency scaling for Mid-Atlantic Ridge earthquakes also can be demonstrated using the distribution of acoustic magnitudes, or source levels. Although fractal seismic behavior has been linked to the structure of the underlying fault population in other environments, power-law fault size distributions have not been observed widely in the mid-ocean ridge setting.

© 2003 Elsevier B.V. All rights reserved.

Keywords: Fractals; Seismic clustering; T-waves; Allan factor; Coefficient of variation

1. Introduction

Numerous natural systems have been shown to exhibit scale-invariant spatial properties (e.g. Turcotte, 1992). Within the field of seismology, the most famous

example of this behavior is the power-law relationship describing the frequency distribution of earthquake sizes (Gutenberg and Richter, 1944). Earthquakes, as well as other natural phenomena, also exhibit temporal fluctuations characterized by a power spectral density $P(f)$ that decays as $1/f^\alpha$; this is sometimes referred to as $1/f$ noise (Bak et al., 1987; Lowen and Teich, 1993; Bittner et al., 1996). Such scaling is consistent with the concept of self-organized criticality, which describes

* Corresponding author. Tel.: +1-845-365-8382;

fax: +1-845-365-8168.

E-mail address: del@ldeo.columbia.edu (D.R. Bohnenstiehl).

the tendency of some systems to evolve spontaneously toward a critical state with no characteristic time or length scale (Bak et al., 1987; Sornette and Sornette, 1988; Bak and Tang, 1989).

The power spectral density provides a measure of how the power in a process is distributed within various frequency bands. For a point-process, such as a sequence of earthquakes, the exponent α characterizes the nature of the time fluctuations. When $\alpha \approx 0$, temporal fluctuations are purely random, as expected for Poisson-like process. For $\alpha > 0$, the distribution of inter-event times displays a power-law clustering behavior, with α measuring the strength of the clusterization (Telesca et al., 2002). In recent years, several regional-scale studies have focused on describing time fluctuations in natural seismic systems (Bittner et al., 1996; Lapenna et al., 2000; Telesca et al., 2000a,b, 2001b). In addition to elucidating the dynamics of the seismic process, these studies have proven useful in discriminating different tectonic regimes (Lapenna et al., 2000; Telesca et al., 2001c) and in monitoring the subsurface movement of magma and stress conditions within the shallow lithosphere (De Rubeis and Tosi, 1997; Barbano et al., 2000; Vinciguerra et al., 2001).

The general tendency for earthquakes to occur in clusters has long been noted within the mid-ocean ridge setting (Sykes, 1970; Francis and Porter, 1971; Bergman and Solomon, 1990). In their statistical analysis of teleseismically-recorded earthquakes, Francis and Porter (1971) have demonstrated that a purely random model cannot describe adequately the distribution of inter-event times and distances along some regions of the ridge crest. They noted also that the proportion of clustered events was tied tightly to the variable detection capabilities of existing seismic networks, a finding which made comparative studies difficult. With regard to seismic clustering, little subsequent progress has been made in this setting and the nature of mid-ocean ridge earthquake distributions has yet to be described fully. This is due in large part to the limited location accuracy and high magnitude of completeness (typically ~ 4.5 – 4.7 M) provided by teleseismic observations and the limited duration and spatial extent of most ocean-bottom seismometer (OBS) studies. Nonetheless, understanding the clustering properties of ridge seismicity remains critical in assessing the impact and interaction of tectonic processes on

other aspects of the ridge system—particularly its hydrothermal, biological and magmatic components (e.g. Sohn et al., 1998; Dziak and Johnson, 2002).

This study examines the size-frequency distribution and time-clustering behavior of earthquakes that occur along the normal faults associated with the plate boundary zone of the slow-spreading Mid-Atlantic Ridge (MAR) (Fig. 1). We utilize an earthquake catalog generated from the detection of seismically-generated Tertiary (T)-waves recorded by autonomous underwater hydrophones (AUHs) moored within the ocean's Sound Fixing And Ranging (SOFAR) channel (Smith et al., 2002). This catalog has a completeness level of ~ 3.0 M (Bohnenstiehl et al., 2002) and therefore represents a substantial improvement relative to the detection capabilities of land-based seismic stations. Moreover, the array overcomes the spatial and temporal limitations imposed by existing OBS datasets—being deployed continuously between 15 and 35°N during the period February 1999 to February 2001.

2. T-waves and hydroacoustic data processing

T-waves represent seismically-generated acoustic energy that propagates efficiently within the oceanic water column's sound velocity minimum, known as the SOFAR channel (Fig. 2) (Tolstoy and Ewing, 1950). Two broad classes of T-waves have been identified. One type is produced within regions of shallow sloping bathymetry in association with earthquakes beneath oceanic islands, continental shelves and subduction zones (e.g. Shurbet and Ewing, 1957; Johnson and Northrup, 1968). In these settings, T-wave generation may involve significant pre-conversion seismic paths between the hypocenter and hydroacoustic source region. Moreover, the signal may exhibit a multipath behavior that is expressed by multiple peaks within the arrival; these peaks are associated with distinct bathymetric promontories that serve as separate T-wave radiators (Shurbet and Ewing, 1957; Johnson and Northrup, 1968; Walker et al., 1992). As a result, the hydroacoustically-derived location of a slope-generated T-wave need not reflect the earthquake's epicenter.

A second type of T-wave has been described in association with shallow hypocenter earthquakes

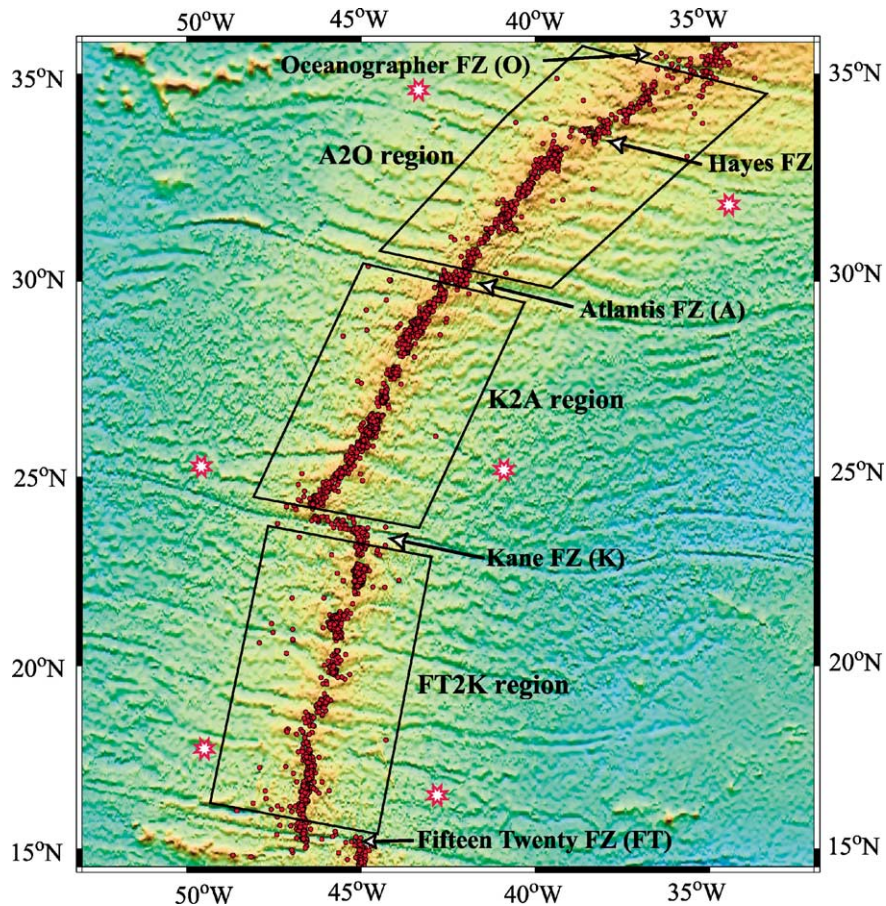


Fig. 1. Bathymetric map of the north-central Mid-Atlantic Ridge. T-wave epicenters within 2° of the ridge axis are shown as red dots. Boxes outline the three sections of the spreading axis in which the temporal pattern of seismicity is examined. Stars indicate the positions of autonomous underwater hydrophones used in monitoring this region.

in the deeper-ocean or abyssal environment (e.g. Johnson et al., 1968; Fox et al., 1994). Unlike their slope-generated counterparts, abyssal T-waves are characterized by a more symmetric coda (Fig. 2), and the locations derived from these signals have been shown to reflect earthquake epicenters closely. For example, observations in the mid-ocean ridge setting have demonstrated sufficient accuracy to lead field parties to sites of active volcanism (e.g., Fox, 1995; Dziak and Fox, 1999) and to associate seismicity with specific structural features on the seafloor (e.g. Fox and Dziak, 1999; Dziak et al., 2000; Caplan-Auerbach et al., 2001; Bohnenstiehl et al., 2002).

The physics of T-wave generation remains an active field of research. In regions of shallow sloping

bathymetry, T-waves often have been attributed to downslope propagation (e.g. Talandier and Okal, 1998). In this formulation, acoustic energy, which is refracted nearly vertically as it enters the water column, becomes trapped and propagates horizontally within the sound channel following a series of reflections between the sloping seafloor and the sea surface. As an alternative, excitation through scattering from a rough seafloor has been proposed as a mechanism for generating T-waves (de Groot-Hedlin and Orcutt, 1999, 2001; Park et al., 2001). This mechanism can be used to model not only slope-derived T-waves, but also the abyssal signals that are not explained readily by downslope propagation.

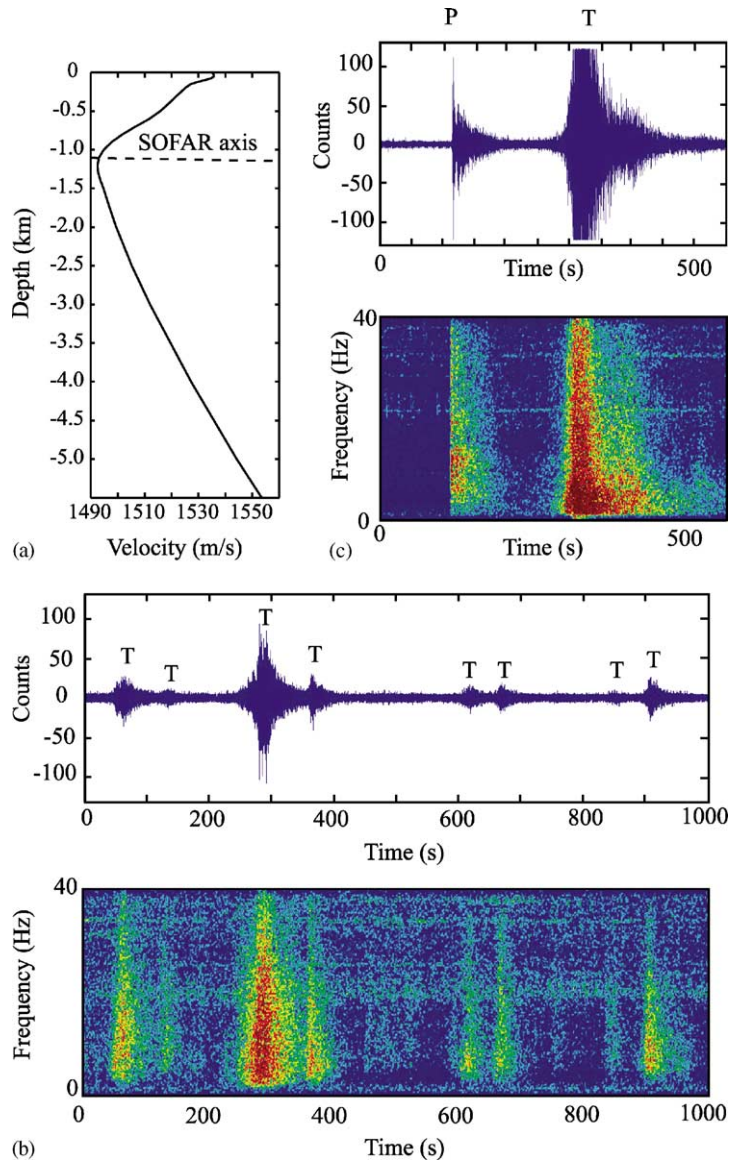


Fig. 2. (a) Atlantic sound velocity profile at latitude 25°N, extracted from GDEM. Hydrophone sensors are floated near the axis of the SOFAR channel. (b) Example T-wave arrivals associated with a series of small (not detected by land-based seismic stations) earthquakes. T-waves are characterized by emergent arrivals, with peak amplitude and coda. Spectrograms calculated within 5 s windows with 75% overlap. (c) Example of a P- and T-wave arrival associated with 3.8 m_b earthquake recorded at a distance of 3.5°. The more impulsive nature of P-wave arrivals distinguishes them easily from T-waves. For large magnitude events, the T-wave signal is often clipped on some or all of the hydrophone sensors, making it difficult to define an empirical relationship between SL and magnitude.

Presently, no depth or focal mechanism information is recovered from the T-wave signal. Recent models, however, have shown that the efficiency of abyssal T-wave generation through scattering should

exhibit mechanism dependence, with strike-slip events being more efficient at generating T-waves than dip-slip events (Park et al., 2001). This has been confirmed observationally using Sound SURveillance

System (SOSUS) data from the northeast Pacific region (Dziak, 2001) and suggests that dip-slip and strike-slip earthquakes should be considered separately when evaluating the T-wave record.

In early 1999, an array of six AUHs was moored on the flanks of the MAR between ~ 15 and 35°N , presenting an opportunity to detect and locate moderate-size, shallow-hypocenter earthquakes within this active plate boundary region (Smith et al., 2002). Each instrument consists of a single hydrophone sensor floated within the sound channel axis at a depth of ~ 800 – 1100 m and tethered via an acoustic release to a seafloor anchor. The recording package consists of a filter/amplifier stage designed to prewhiten the ambient noise spectrum, an accurate (<1 s per year drift) clock that is GPS-synchronized prior to deployment, a logging computer, and multiple hard disks for data storage. The systems deployed within the Atlantic were programmed to record 1-byte resolution at a sample rate of 110 Hz. Recovered and processed data from February 1999 to February 2001 are considered within this paper. This monitoring effort is ongoing, with annual turn-around cruises to recover and redeploy the instruments. Future deployments will involve instruments with increased sampling rate and resolution.

Following an analyst's identification of T-wave arrivals, an epicentral (source region) location and origin time are derived using an iterative nonlinear least-squares method that minimizes the squared differences between the predicted and recorded arrival times at each instrument, as described in Fox et al. (2001). Hydroacoustic travel times are calculated within a sound speed model derived from the Generalized Digital Environmental Model (GDEM) (Teague et al., 1990). To minimize bias associated with the width of the T-wave source region, the peak energy of the T-wave signal is used as the arrival time in locating submarine earthquakes. The correlation of event depth and rise time in the abyssal setting suggests that this portion of the signal radiates from the near epicentral region, where the amplitude of the scattered energy is largest (Dziak et al., 1995; Slack et al., 1999). Point-source Monte Carlo simulations suggest an epicentral accuracy of <4 km in latitude and longitude (95% confidence level) for events within the array (Fox et al., 2001; Smith et al., 2002); however, it should be noted that the abyssal T-wave likely is generated over a region of many km^2 .

After each event is located, an independent estimate of the acoustic magnitude, or source level (SL), is calculated for each receiving hydrophone by adding a transmission loss factor that accounts for both spherical spreading from the seafloor into the sound channel and cylindrical spreading along the sound channel path (Fox et al., 2001). Source levels are measured in decibels relative to μPa at 1 m (dB re μPa @ 1 m) (Dziak et al., 1997; Dziak, 2001; Fox et al., 2001). (Note: The instrument response calibration and SL estimates have been adjusted $+5$ dB relative to those published in earlier studies using the MAR hydrophone array (Smith et al., 2002; Bohnenstiehl et al., 2002)).

3. Geology and seismicity of the North-Central Mid-Atlantic Ridge

The MAR from 15 to 35°N is a slow-spreading (~ 15 mm per year half-rate), divergent plate boundary marked by a 1.5 – 3 km deep, 15 – 30 km wide axial rift valley. In the northern section of this region, the ridge axis becomes noticeably shallower and broader, reflecting the influence of the Azores hotspot near 39°N (Fig. 1). The ridge axis is offset by five major transform faults—the Fifteen-Twenty, Kane, Atlantis, Hayes and Oceanographer (Fig. 1). Between the transforms, the ridge is divided into smaller second-order spreading segments whose ends are defined by non-transform offsets (Sempere et al., 1990; Spencer et al., 1997).

At slow-spreading ridges, most of the active plate separation is accommodated by the accretion of new lithosphere, with an additional 10 – 20% accommodated by extensional brittle deformation. Studies of seismic coupling, defined as the ratio of the seismic moment release to the geometric moment release inferred from faulting studies, indicate values near 1.0 for normal faults along the MAR (Solomon et al., 1988; Cowie et al., 1993; Sobolev and Rundquist, 1999). The frequency of volcanic events is unknown within this region; however, near-bottom surveys indicate that much of the rift valley floor shows evidence of recent volcanism (e.g. Ballard and van Aldel, 1977; Smith and Cann, 1993).

Morphologic observations, such as sonar imagery and near-bottom photography, suggest that active extensional faulting does not extend beyond the crest

of the rift valley walls in the slow-spreading environment (e.g. McAllister and Cann, 1996; Searle et al., 1998). This is confirmed by the spatial distribution of T-wave epicenters, which indicates that most earthquakes occur within 15–20 km of the axis (Smith et al., 2002). Although many extensional fault populations exhibit power-law size frequency distributions (Scholz, 2002), such scaling has not been observed widely along the MAR or within other mid-ocean ridge settings (e.g. Cowie et al., 1993, 1994; Carbotte and Macdonald, 1994; Escartin et al., 1999; Bohnenstiehl and Carbotte, 2001). Therefore, mid-ocean ridge earthquake studies may present an opportunity to assess the impact of the underlying fault population on the scaling and dynamics of seismicity. Studies in other environments have suggested a link between the scale-invariant behavior of seismicity and the fractal nature of the underlying fault population (e.g. Guo and Ogata, 1997; Scholz, 1998; Nanjo et al., 1998; Sherman and Gladkov, 1999; Nanjo and Nagahama, 2000).

The 15–35°N region has been the site of numerous short-term OBS experiments that have been focused primarily within the median rift valley (e.g. Huang et al., 1986; Toomey et al., 1988; Kong et al., 1992; Wolfe et al., 1995; Barclay et al., 2001). Some of these OBS studies indicate variability in the depth of the seismogenic zone at the second-order segment scale, with the maximum depth of seismicity becoming deeper (~8–10 km) near the segment ends and shallower (~6–8 km) near the segment center in response to higher crustal temperatures and presumably increased magmatism (Kong et al., 1992). At a regional scale, there also is evidence that the maximum depth of seismicity shallows toward the Azores hot spot, again reflecting hotter lithospheric temperatures and increased magmatism (Barclay and Toomey, 2001). Focal mechanisms indicate dominantly normal faulting events along spreading centers and strike-slip events along the transforms (e.g. Huang et al., 1986; Bergman and Solomon, 1984; Kong et al., 1992).

4. Data selection, completeness level and size-frequency distribution

To avoid complications associated with the mechanism-dependent efficiency of T-wave genera-

tion (Dziak, 2001; Park et al., 2001), focus is given to spreading-center (normal-faulting) earthquakes, which represent the vast majority of the events in the region. Three sections of the spreading axis with a similar number of earthquakes and a similar spatial dimension are considered, as defined by the Fifteen-Twenty, Kane, Atlantis and Oceanographer Transforms (Fig. 1). The short-offset Hayes fracture zone, which produces relatively few earthquakes of detectable size over the period of observation, is incorporated into the northern Atlantis-to-Oceanographer section. Earthquakes within two degrees of the spreading axis and more than 0.2 degrees from the transforms are considered.

Studying these three regions presents an opportunity to determine if the temporal pattern of earthquake production is influenced by regional scale changes in thermal structure and magmatic budget, factors influenced by proximity to the Azores hot spot. The temporal scaling of transform seismicity is not considered due to difficulties in assigning a mechanism to events near the ridge-transform intersection (e.g. Wilcock et al., 1990), and because the number of events along most of the transforms is too small to allow for a robust analysis.

The cumulative SL-frequency distribution of earthquakes within each region is shown in Fig. 3. These data are consistent with a size-frequency distribution of the form:

$$\log_{10} N(\text{SL}) = a - b_t \text{SL}, \quad (1)$$

where N is the cumulative number of events having source level greater or equal to SL, a reflects the total number of events, and b_t is the log-linear slope of the data (Bohnenstiehl et al., 2002). Since the decibel SL scale is a logarithmic measure of earthquake size, Eq. (1) is analogous to the Gutenberg–Richter relationship and consistent with a power-law distribution of earthquake size or moment (Gutenberg and Richter, 1944).

The parameters a and b_t and the completeness level of the data (M_c) are estimated simultaneously by generating a series of synthetic distributions that follow Eq. (1). These synthetics represent a least squares fit to the data, each calculated using a different minimum SL thresholds. To measure the goodness-of-fit for each synthetic, the absolute difference between the number of observed and synthetic events (normalized

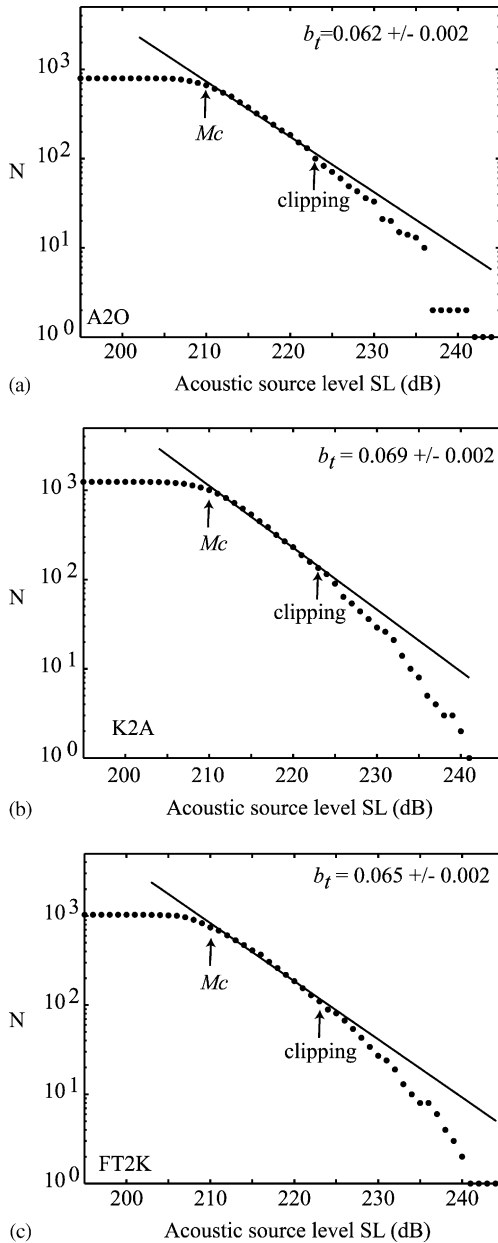


Fig. 3. Cumulative SL-frequency distribution of epicenters within the three regions studied, (a) A2O; (b) K2A; (c) FT2K. Solid lines indicate a least-squares fit to the data between the completeness level M_c (210 dB or $\sim 3.0M$ for all regions) and clipped values (223 dB). Data exhibit similar b_1 within each region. Decibels are referenced to $1 \mu\text{Pa}$ at a distance of 1 m. Note that the instrument response calibration has been adjusted relative to our earlier studies using the MAR hydrophone array (Smith et al., 2002; Bohnenstiehl et al., 2002), resulting in a 5 dB increase in all SL estimates. This does not influence the conclusions of these earlier studies.

by the observed number) is calculated in each SL bin and summed. As the minimum SL threshold is increased, the parameters a and b_1 are selected when the residual first drops below a critical value (0.05). The completeness level of the data is defined as the minimum SL threshold for which this critical residual value is reached. This is an adaptation of an empirical method commonly used in evaluating seismic catalogs (Wiemer and Wyss, 2000) and an improvement over the subjective determination we have implemented previously (Bohnenstiehl et al., 2002). Due to clipping of the hydrophone sensors during large magnitude earthquakes, we exclude events having $SL > 223$ dB from this analysis.

Within all three regions, the data are complete for events ≥ 210 dB. Fitting the data between 210 and 223 dB, b_1 values of 0.062 ± 0.002 , 0.069 ± 0.002 and 0.065 ± 0.002 are found within the Atlantis-to-Oceanographer (A2O), Kane-to-Atlantis (K2A) and Fifteen-Twenty-to-Kane (FT2K) regions, respectively. These observations are consistent with a relatively uniform detection capability across the array and suggest that the efficiency of T-wave generation does not vary significantly between these regions. The 210 dB level is equivalent to a completeness level of approximately magnitude 3.0, based on the number of events observed and an extrapolation of the teleseismic size-frequency distribution (Bohnenstiehl et al., 2002).

In investigating the clustering properties of seismicity, we consider only events ≥ 210 dB—leaving 640 (A2O), 961 (K2A) and 716 (FT2K) events within each of the three regions. When normalized for the length of the plate boundary, these values are equivalent to approximately 69, 125 and 78 events/degree in the respective regions. It is noteworthy that the rate of AUH-detectable seismicity on the MAR is more than two orders of magnitude greater than that observed on the fast-spreading East Pacific Rise (e.g. Fox et al., 2001), where the presence of a thin seismogenic layer limits the production of moderate to large size earthquakes (Cowie et al., 1993).

5. Describing the time-clustering properties of seismicity

A sequence of earthquakes can be represented as a series of point process events centered at each

earthquake's occurrence time (e.g. Telesca et al., 2002). Using this representation, the time distribution of events can be expressed as a set of inter-event times, and the tendency for earthquakes to cluster is then described by the coefficient of variation (C_v) (Kagan and Jackson, 1991). C_v is defined as the standard deviation of the inter-event times divided by the mean inter-event time, and takes a value of 0, 1 and >1 , for a periodic, Poissonian (completely random) and clustered process, respectively (Kagan and Jackson, 1991). Although this parameter is useful in describing the sequence as clustered or not clustered, it does not identify the timescales involved.

The clustering properties of the sequence also can be investigated by examining the correlation among blocks of inter-event times using range/standard deviation (R/S) analysis, more commonly known as rescaled range analysis (Hurst et al., 1965; Mandelbrot and Wallis, 1969). Consider a block of m inter-event times ($\varepsilon(i)$) ($i = 1, 2, 3, \dots, m$). The accumulated departure of each inter-event time from the average is given by:

$$x(i, m) = x(i) - i\langle\varepsilon\rangle_m, \quad (2)$$

where $x(i)$ is the cumulative inter-event time and $\langle\varepsilon\rangle_m$ the mean inter-event time within the m event block (Telesca et al., 2002). The range R of these accumulated departures can be written as:

$$R(m) = \max_{1 < i < m} x(i, m) - \min_{1 < i < m} x(i, m). \quad (3)$$

To compare the range of sequences with different scales, $R(m)$ is divided by the standard deviation, $S(m)$. Calculating R/S for a range of m and fitting R/S against m , $R/S \propto m^H$ (Hurst's rule), yields an estimate of the Hurst exponent H (Hurst et al., 1965). For $H > 0.5$, a positive correlation exists among intervals, or there is a tendency for the local trend to persist—with larger values of H indicating greater persistence. For $H < 0.5$, a negative correlation exists between intervals, or the series demonstrates antipersistence. For $H = 0.5$, no correlation exists between intervals. H can be related to the power spectral density exponent, with $\alpha = 2H - 1$ (Barton and Poor, 1988).

Counting statistics, such as Allan factor analysis, represent an alternative to the inter-event time representation utilized by C_v and R/S analysis. Allan factor (AF) analysis also can be used to recognize power-law behavior in a point process and provides an established

method for estimating the exponent of the power spectral density function (Thurner et al., 1997; Telesca et al., 2002). Here, the time axis is divided into equally spaced contiguous counting windows of duration τ , yielding a sequence of counts $N_k(\tau)$ representing the number of events within each window. The AF is defined as the variance of successive counts for a given counting time divided by twice the mean number of events in that counting time (Allan, 1966; Barnes and Allan, 1966).

$$\text{AF}(\tau) = \frac{\langle(N_{k+1}(\tau) - N_k(\tau))^2\rangle}{2\langle N_k(\tau)\rangle}. \quad (4)$$

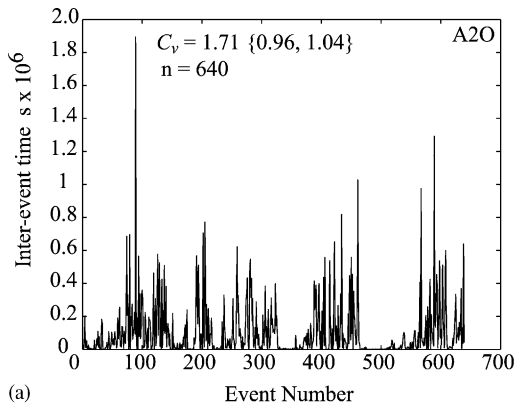
For a fractal point process where $P(f)$ scales as $1/f^\alpha$, $\text{AF}(\tau) = 1 + (\tau/\tau_1)^\alpha$ (Thurner et al., 1997). For α close to zero, the occurrence of earthquakes is random; whereas $\alpha > 0$ indicates a power-law scaling that describes the temporal clustering of events. Larger α indicates a stronger degree of clustering. τ_1 is known as the fractal onset time and marks the lower limit of significant scaling behavior.

6. Time clustering observations and results

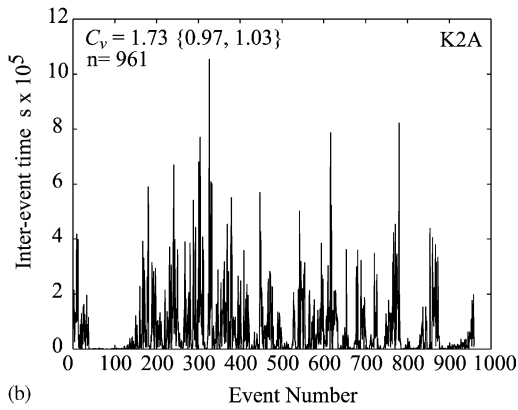
The inter-event times within each of the regions are shown in Fig. 4 and range from $\sim 10^2$ to 10^6 s, with mean inter-event times of 1.1×10^5 , 0.67×10^5 and 0.91×10^5 s for the A2O, K2A and FT2K regions, respectively. In all three regions C_v is greater than 1.0, with values of 1.71 (A2O), 1.73 (K2A) and 1.34 (FT2K). This indicates a clustered time distribution for $\text{SL} \geq 210$ dB (~ 3.0 M) earthquakes along the MAR axis.

R/S analysis of inter-event times indicates monotonically increasing behavior, with $H = 0.79 \pm 0.02$ (A2O), 0.78 ± 0.01 (K2A) and 0.68 ± 0.02 (FT2K) (Fig. 5). Predicted values of α are 0.58, 0.56 and 0.36. This behavior reflects a positive correlation between intervals and indicates that the process is persistent—meaning that long (or short) inter-event times are more likely to be followed by long (or short) inter-event times.

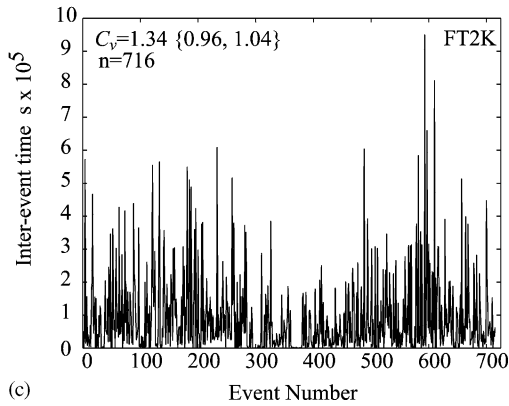
The AF also increases monotonically for counting times $\gtrsim 5 \times 10^3$ s (Fig. 6). At counting times $\lesssim 5 \times 10^3$ s the clustering properties become negligible and the AF takes a value near unity. Values of 0.38 ± 0.02 , 0.55 ± 0.07 and 0.12 ± 0.03 are obtained for α (Fig. 6). The



(a)

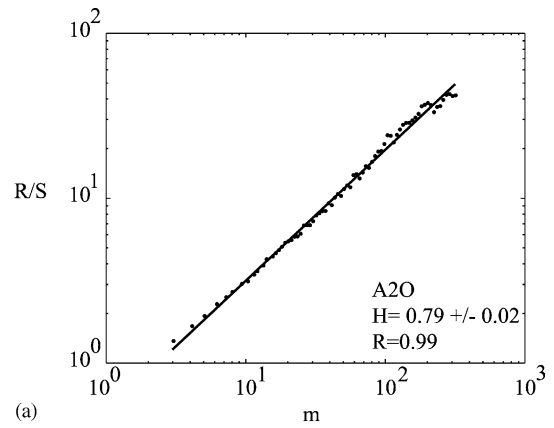


(b)

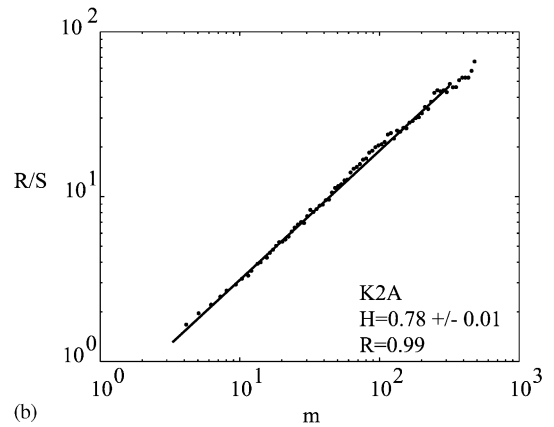


(c)

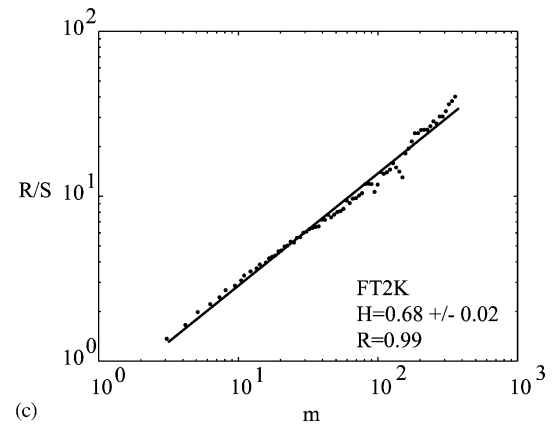
Fig. 4. Inter-event times ($\varepsilon(i)$) vs. event number (i) within the (a) A2O; (b) K2A; (c) FT2K regions. Note variable scale of axes. Small inter-event times indicate periods when earthquakes occur closely spaced in time. Large inter-event times indicate a slower rate of earthquake production. Within each region, C_v is greater significantly than 1.0, indicating a clustered behavior. Bracketed numbers represent $1 - \sigma C_v$ limits for a Poisson distribution, based on 1000 simulations of a random sequence using the total event number and mean event rate observed in each region.



(a)



(b)



(c)

Fig. 5. Range/standard deviation (R/S) vs. inter-event block size (m) within the (a) A2O; (b) K2A; (c) FT2K regions. $H > 0.5$ indicates persistence of the time series.

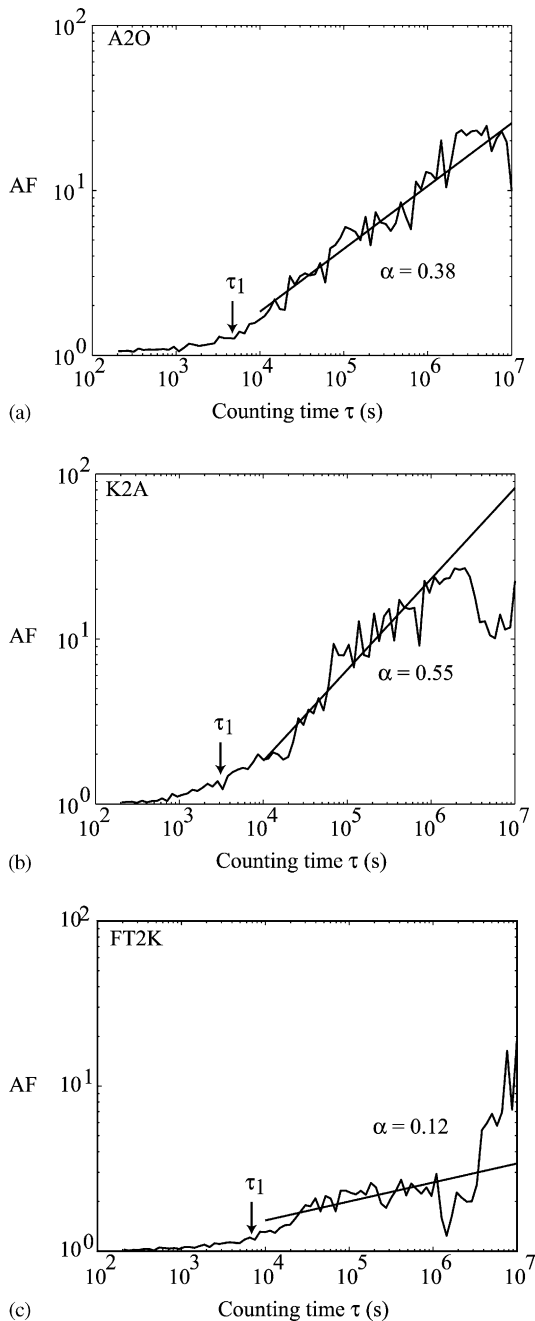


Fig. 6. Allan factor (AF) vs. counting window length (τ) within the (a) A2O; (b) K2A; (c) FT2K regions. τ_1 indicates the fractal onset time, which is approximately $\sim 5 \times 10^3$ in each region.

discrepancy between these values and those estimated using R/S analysis probably reflects the slow convergence properties of the R/S method and the moderate ($N = 640\text{--}961$) length of the time series examined (Bassingthwaite and Raymond, 1994). Evaluation of the AF method by Telesca et al. (2000a, 2001b) suggests a better performance of this estimator, and so the α values determined using the AF method are preferred.

Fig. 7 shows the AF data estimated with different SL thresholds applied to the catalog. The value of α generally decreases as the SL thresholds are increased, ranging from 0.38 to 0.15 (A2O), 0.55 to 0.25 (K2A) and 0.12 to 0.0 (FT2K) for thresholds of 210–224 dB. In the FT2K region, the distribution of events can be considered random ($\alpha \approx 0$) for thresholds ≥ 222 dB (approximately). At all threshold values, α remains larger in the K2A and A2O regions than in the FT2K region.

To examine the correlation between seismic clustering and other temporal phenomena, C_v is shown in Fig. 8 as a function of time, as calculated using 50-earthquake windows that are offset by 10 earthquakes in time. C_v varies between approximately 1–5 (A2O), 1–3 (K2A) and 1–1.5 (FT2K). The time distribution of events may be described as random for periods of several tens of days within all three regions. This is shown by the solid horizontal lines in Fig. 8, which represent the $1 - \sigma$ range of C_v for a simulated 50-event random sequence with the same mean event rate as the data.

Fig. 8 also shows the time-magnitude distribution of earthquakes recorded at teleseismic distances. Many of the largest C_v values are correlated in time with large magnitude earthquakes. The dominant peak within the A2O region and the largest windowed C_v value within any of the regions studied ($C_v = 5.2$) corresponds to a 6.1 Ms mainshock near $31^\circ 30'N$ and reflects the clustering of subsequent aftershock activity. Two near-equal C_v peaks occur within the K2A region of the MAR. The first peak, near day 100, is associated with a 5.9 Mw mainshock near $24^\circ 30'N$. The ensuing aftershock sequence was the largest recorded during the first 2 years of acoustic monitoring in the Atlantic, containing ~ 165 events (Bohnenstiehl et al., 2002). The second peak, near day 800, is not associated with any large magnitude teleseismic events. Instead, this period of clustered

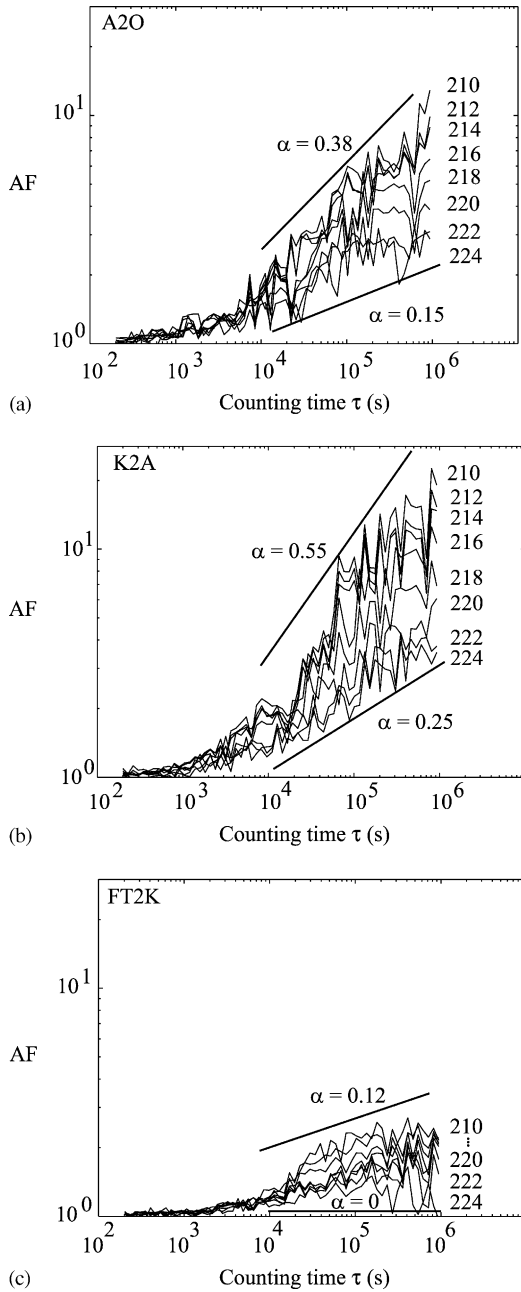


Fig. 7. Allan factor (AF) vs. counting window length (τ) within the (a) A2O; (b) K2A; (c) FT2K regions with various SL thresholds applied to the catalog.

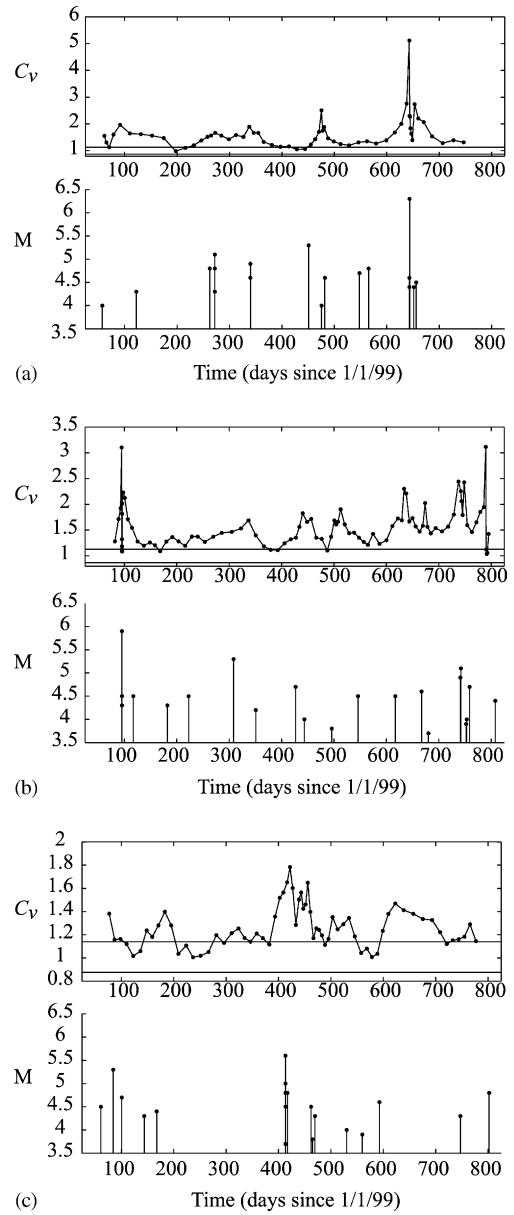


Fig. 8. (Top panels) Coefficient of variation (C_v) calculated within 50-event moving windows offset by 10 events in time within the (a) A2O; (b) K2A; (c) FT2K regions. Horizontal lines show $1 - \sigma$ C_v limits for a Poisson distribution, based on 1000 50-event simulations using the mean event rate observed within each region. (Lower panels) Magnitude (M)–time history of earthquakes within the Preliminary Determination of Epicenters catalog for the (a) A2O; (b) K2A; (c) FT2K regions.

activity reflects a large seismic swarm (lacking a well-defined mainshock) that occurred along the Broken Spur Segment (Searle et al., 1998) near 29°N. The largest peak within the FT2K region ($C_v = 1.8$) corresponds to a 5.5 Mw mainshock event and related aftershock activity (Bohnenstiehl et al., 2002).

7. Summary and conclusions

A catalog of earthquakes derived from the detection of seismically generated T-waves has been used to examine the time-clustering behavior and size-frequency distribution of north-central MAR earthquakes. During the 2-year period of observation, the time distribution of ≥ 3.0 M (approximately) earthquakes can be described as a non-periodic, non-random, clustered phenomenon, with coefficient of variation (C_v) > 1.0 . When C_v is examined within windows of constant event number, temporal spikes, which indicate an increase in the strength of the clusterization, are observed. These increases are correlated with mainshock-aftershock sequences and swarm activity (more typically the former) and therefore represent a response to large magnitude earthquakes and/or possibly magmatic processes.

Both rescaled-range (R/S) and Allan factor (AF) analysis reveal a fractal time clustering behavior for MAR earthquakes. This is consistent with seismic observations within a number of terrestrial environments (e.g. Lapenna et al., 2000; Telesca et al., 2000a,b, 2001a). Using the AF method, the power-law exponent α is estimated to be 0.36, 0.55 and 0.12 for the Atlantis-to-Oceanographer, Kane-to-Atlantis, and Fifteen-Twenty-to-Kane regions, respectively. A fractal onset time of $\sim 5 \times 10^3$ s is observed within each region. A decrease in α is observed as the data are filtered to higher SL thresholds, with a random ($\alpha \approx 0$) distribution observed in the southern-most Kane-to-Atlantis region when thresholds ≥ 222 dB (approximately) are applied. Although hot spot influenced changes in thermal structure and magmatic budget might be expected to impact the long-term pattern of earthquake production, the power-law exponent α does not vary systematically with proximity to the Azores. The least clustered behavior (smallest C_v and α), however, occurs in the most distant Fifteen-Twenty-to-Kane region.

The acoustic source level, measured in decibels, scales in a manner analogous to the well-known Gutenberg Richter relationship. This agrees with the results of previous teleseismic and OBS studies in the mid-ocean ridge setting (e.g. Francis, 1986; Solomon et al., 1988; Toomey et al., 1988; Kong et al., 1992) and implies a power-law size (moment)-frequency distribution for north-central MAR earthquakes. The scale-invariant behavior exhibited by the size-frequency distribution and time-fluctuations is consistent with the description of seismicity as self-organized critical phenomena (e.g. Sornette and Sornette, 1988; Bak and Tang, 1989; Bittner et al., 1996).

In other settings, it has been suggested that fractal seismic behavior may be tied closely to the fractal structure of fault populations (e.g. Guo and Ogata, 1997; Scholz, 1998; Nanjo et al., 1998; Sherman and Gladkov, 1999; Nanjo and Nagahama, 2000); however, a power-law distribution of fault sizes has not been recognized widely within the mid-ocean ridge setting (Cowie et al., 1993, 1994; Carbotte and Macdonald, 1994; Escartin et al., 1999; Bohnenstiehl and Carbotte, 2001). If the proposed link between fault and earthquake scaling relationships is valid, a seismically active subset of the mapped fault populations must display a power-law size frequency distribution (cf. Cowie et al., 1993; Bohnenstiehl and Kleinrock, 1999). Alternatively, our observations imply that fractal seismic behavior may arise when the structure of the fault system is not power-law in nature.

Acknowledgements

Hydroacoustic data collection was facilitated by NSF grant #OCE-9811575. D.R.B. was supported partially by the Department of Earth and Environmental Sciences at Columbia University. Helpful discussions with S. Carbotte, Z. Karcz and C. Scholz are gratefully acknowledged. M. Fowler, P. Will and J. Haxel processed much of the raw hydroacoustic data used in this study; M. Fowler's efforts at sea were critical to the successful recovery and deployment of the AUH instruments. Hardware and software developed by H. Matsumoto and A. Lau, respectively, have made this work possible. Comments by J. Caplan-Auerbach and an anonymous reviewer were very helpful in revising

this manuscript. Contribution numbers: PMEL-2520, WHOI-10897 and LDEO-6450.

References

- Allan, D.W., 1966. Statistics of atomic frequency standards. *Proc. IEEE* 54, 221–230.
- Bak, P., Tang, C., 1989. Earthquakes as a self-organized critical phenomenon. *J. Geophys. Res.* 94, 15,635–15,637.
- Bak, P., Tang, C., Wiesenfeld, K., 1987. Self-organized criticality: an example of $1/f$ noise. *Phys. Rev. Lett.* 59, 381–384.
- Ballard, R.D., van Aldel, T.H., 1977. Morphology and tectonics of the inner rift valley at lat $36^{\circ}50'N$ on the Mid-Atlantic Ridge. *Geol. Soc. Am. Bull.* 88, 507–530.
- Barbano, M.S., De Rubeis, V., Tosi, P., Vinciguerra, D., 2000. Clustering properties of Etna seismicity during 1981–1991. *J. Seismol.* 4, 191–196.
- Barclay, A.H., Toomey, D.R., Solomon, S.C., 2001. Microearthquake characteristics and crustal V_p/V_s structure at the Mid-Atlantic Ridge $35^{\circ}N$. *J. Geophys. Res.* 106, 2017–2034.
- Barnes, J.A., Allan, D.W., 1966. A statistical model of flicker noise. *Proc. IEEE* 54, 176–178.
- Bassingthwaighe, J.B., Raymond, G.M., 1994. Evaluating rescaled-range analysis for time series. *Annal. Biomed. Eng.* 22, 432–444.
- Barton, R.J., Poor, H.V., 1988. A statistical model for flicker noise. *Proc. IEEE* 54, 221–230.
- Bittner, H.R., Tosi, P., Braun, C., Meesmann, M., Kniffki, K.D., 1996. Counting statistics of f^B fluctuations: a new method for the analysis of earthquake data. *Geol. Rundsch.* 85, 110–115.
- Bergman, E.A., Solomon, S.C., 1984. Source mechanisms of earthquakes near mid-ocean ridges from body waveform inversion; implications for the early evolution of oceanic lithosphere. *J. Geophys. Res.* 89, 11,415–11,441.
- Bergman, E.A., Solomon, S.C., 1990. Earthquake swarms of the Mid-Atlantic Ridge: products of magmatism or extensional tectonics. *J. Geophys. Res.* 95, 4943–4965.
- Bohnenstiehl, D.R., Kleinrock, M.C., 1999. Faulting and fault scaling on the median valley floor of the Trans-Atlantic Geotraverse (TAG) segment, $\sim 26^{\circ}N$ on the Mid-Atlantic Ridge. *J. Geophys. Res.* 104, 29,351–29,364.
- Bohnenstiehl, D.R., Carbotte, S.M., 2001. Faulting patterns near $19.5^{\circ}S$ on the East Pacific Rise: implications for fault formation and growth at superfast-spreading centers. *Geochem. Geophys. Geosyst.* 2, 2001GC000156.
- Bohnenstiehl, D.R., Tolstoy, M., Dziak, R.P., Fox, C.G., Smith, D.K., 2002. Aftershocks sequences in the mid-ocean ridge environment: an analysis using hydroacoustic data. *Tectonophysics* 354, 49–70.
- Caplan-Auerbach, J., Fox, C.G., Duennebier, F.K., 2001. Hydroacoustic detection of submarine landslides on Kilauea volcano. *Geophys. Res. Lett.* 28, 1811–1813.
- Carbotte, S.M., Macdonald, K.C., 1994. Comparison of seafloor tectonic fabric at intermediate, fast, and super fast spreading ridges; influence of spreading rate, plate motions, and ridge segmentation on fault patterns. *J. Geophys. Res.* 99, 13,609–13,631.
- Cowie, P.A., Scholz, C.H., Edwards, M., Malinverno, A., 1993. Fault strain and seismic coupling on mid-ocean ridges. *J. Geophys. Res.* 98, 17,911–17,920.
- Cowie, P.A., Malinverno, A., Ryan, W.B.F., Edwards, M.H., 1994. Quantitative fault studies on the East Pacific Rise a comparison of sonar imaging techniques. *J. Geophys. Res.* 99, 15,205–15,218.
- de Groot-Hedlin, Orcutt, J.A., 1999. Synthesis of earthquake-generated T-waves. *Geophys. Res. Lett.* 26, 1227–1230.
- de Groot-Hedlin, Orcutt, J.A., 2001. Excitation of T-phases by seafloor scattering. *J. Acoust. Soc. Am.* 109, 1944–1953.
- De Rubeis, V., Tosi, P., 1997. Time clustering properties of seismicity in the Etna region between 1874 and 1913. *Geophys. Res. Lett.* 24, 2331–2334.
- Dziak, R.P., 2001. Empirical relationship of T-wave energy and fault parameters of northeast Pacific Ocean earthquakes. *Geophys. Res. Lett.* 28, 2537–2540.
- Dziak, R.P., Fox, C.G., 1999. The January 1998 earthquake swarm at Axial Volcano, Juan de Fuca Ridge: hydroacoustic evidence of seafloor volcanic activity. *Geophys. Res. Lett.* 26, 3429–3432.
- Dziak, R.P., Johnson, H.P., 2002. Stirring the oceanic incubator. *Science* 296, 1406–1407.
- Dziak, R.P., Fox, C.G., Schreiner, A.E., 1995. The June–July 1993 seismo-acoustic event at CoAxial segment, Juan de Fuca Ridge; evidence for a lateral dike injection. *Geophys. Res. Lett.* 22, 135–138.
- Dziak, R.P., Fox, C.G., Matsumoto, H., Schreiner, A.E., 1997. The April 1992 Cape Mendocino earthquake sequence; seismo-acoustic analysis utilizing fixed hydrophone arrays. *Mar. Geophys. Res.* 19, 137–162.
- Dziak, R.P., 2000. Recent tectonics of the Blanco Ridge, eastern Blanco transform fault zone. *Marine Geophys. Res.* 21, 423–450.
- Escartin, J., Cowie, P.A., Searle, R.C., Allerton, S., Mitchell, N.C., MacLeod, J.C., Slootweg, A.P., 1999. Quantifying tectonic strain and magmatic accretion at a slow spreading ridge segment, Mid-Atlantic Ridge, $29^{\circ}N$. *J. Geophys. Res.* 104, 10,421–10,437.
- Fox, C.G., 1995. Special collection on the June 1993 volcanic eruption on the CoAxial segment of the Juan de Fuca Ridge. *Geophys. Res. Lett.* 22, 129–130.
- Fox, C.G., Dziak, R.P., 1999. Internal deformation of the Gorda Plate observed by hydroacoustic monitoring. *J. Geophys. Res.* 104, 17603–17615.
- Fox, C.G., Dziak, R.P., Matsumoto, H., Schreiner, A.E., 1994. Potential for monitoring low-level seismicity on the Juan de Fuca Ridge using military arrays. *Mar. Tech. Soc. J.* 27, 22–30.
- Fox, C.G., Matsumoto, H., Lau, T.K.A., 2001. Monitoring Pacific Ocean seismicity from an autonomous hydrophone array. *J. Geophys. Res.* 106, 4183–4206.
- Francis, T.J.G., 1986. Seismicity of mid-oceanic ridges and its relation to properties of the upper mantle and crust. *Nature* 220, 899–901.
- Francis, T.J.G., Porter, I.T., 1971. A statistical study of Mid-Atlantic Ridge earthquakes. *Geophys. J. R. Astron. Soc.* 24, 31–50.

- Guo, Z., Ogata, Y., 1997. Statistical relations between the parameters of aftershocks in time. *J. Geophys. Res.* 102, 2857–2873.
- Gutenberg, B., Richter, C.F., 1944. Frequency of earthquakes in California. *Bull. Seism. Soc. Am.* 34, 185–188.
- Huang, P.Y., Solomon, S.C., Bergman, E.A., Nabelek, J.L., 1986. Focal depths and mechanisms of Mid-Atlantic Ridge earthquakes from body waveform inversion. *J. Geophys. Res.* 91, 579–598.
- Hurst, H.E., Black, R.P., Simaika, Y.M., 1965. Long-term storage: an experimental study. Constable, London.
- Johnson, R.H., Northrup, R.A., 1968. T-wave radiators in the western Aleutians. *Bull. Seismol. Soc. Am.* 58, 1–10.
- Johnson, R.H., Norris, R.A., Duennebieber, F.K., 1968. Abyssally generated T phases. The crust and upper mantle of the Pacific area—International Upper Mantle Project, Science Report 15. Geophysical Monograph. American Geophysical Union, Washington, DC, United States, pp. 70–78.
- Kagan, Y.Y., Jackson, D.D., 1991. Long-term earthquake clustering. *Geophys. J. Int.* 104, 117–133.
- Kong, L.S.L., Solomon, S.C., Purdy, G.M., 1992. Microearthquake characteristics of a mid-ocean ridge along-axis high. *J. Geophys. Res.* 97, 1659–1685.
- Lapenna, V., Macchiato, M., Piscitelli, S., Telesca, L., 2000. Scale-invariance properties in seismicity in Southern Apennine Chain (Italy). *Pure Appl. Geophys.* 157, 589–601.
- Lowen, S.B., Teich, M.C., 1993. Fractal renewal process generates $1/f$ noise. *Phys. Rev. E* 47, 992–1001.
- Mandelbrot, M.B., Wallis, J.R., 1969. Some long run properties of geophysical records. *Water Res. J.* 5, 321–340.
- McAllister, E., Cann, J.R., 1996. Initiation and evolution of boundary-wall faults along the Mid-Atlantic Ridge, 25–29°N. In: MacLeod, C.J., Tyler, T.A., Walker C.L. (Eds.), *Tectonic, Magmatic, Hydrothermal and Biological Segmentation of Mid-Ocean Ridges*. *Geol. Soc. Spec. Publ.* 118, 29–48.
- Nanjo, K., Nagahama, H., 2000. Spatial distribution of aftershocks and the fractal structure of active fault systems. In: Blenkinsop, T.G., Kruhl, J.H., Kupkova, Mirriam (Eds.), *Fractals and Dynamic Systems in Geosciences*. Birkhaeuser Verlag, Basel, Switzerland.
- Nanjo, K., Nagahama, H., Satomura, M., 1998. Rates of aftershock decay and the fractal structure of active fault systems. *Tectonophysics* 287, 173–186.
- Park, M., Odom, R.I., Soukup, D.J., 2001. Modal scattering a key to understanding oceanic T-waves. *Geophys. Res. Lett.* 28, 3401–3404.
- Scholz, C.H., 1998. A further note on earthquake size distributions. *Bull. Seismol. Soc. Am.* 88, 1325–1326.
- Scholz, C.H., 2002. *The Mechanics of Earthquakes and Faulting*, 2nd ed. Cambridge University Press, Cambridge, p. 464.
- Searle, R.C., 1998. Fault structure and detailed evolution of a slow spreading ridge segment the Mid-Atlantic Ridge at 29°N. *Earth Planet. Sci. Lett.* 154, 167–183.
- Sempere, J.C., Purdy, G.M., Schouten, H., 1990. Segmentation of the Mid-Atlantic Ridge between 24°N and 30°40'N. *Nature* 334, 427–431.
- Sherman, S.I., Gladkov, A.S., 1999. Fractals in studies of faulting and seismicity in the Baikal rift zone. *Tectonophysics* 308, 133–142.
- Shurbet, D.H., Ewing, M., 1957. T-waves at Bermuda and transformation of elastic waves. *Bull. Seis. Soc. Am.* 47, 251–262.
- Slack, P.D., Fox, C.G., Dziak, R.P., 1999. P-wave detection thresholds, Pn velocity estimates, and T-wave location uncertainty from oceanic hydrophones. *J. Geophys. Res.* 104, 13,061–13,073.
- Smith, D.K., Cann, J.R., 1993. Building the crust at the Mid-Atlantic Ridge. *Nature* 365, 707–715.
- Smith, D.K., Tolstoy, M., Fox, C.G., Bohnenstiehl, D.R., Matsumoto, H., Fowler, M.J., 2002. Hydroacoustic monitoring of seismicity at the slow-spreading Mid-Atlantic Ridge. *Geophys. Res. Lett.*, 10.1029/2001GL013912.
- Sobolev, P.O., Rundquist, D.V., 1999. Seismicity of oceanic and continental rifts; a geodynamic approach. *Phys. Earth Planet. Inter.* 111, 253–266.
- Sohn, R.A., Fornari, D.J., Von Damm, K.L., Hildebrand, J.A., Webb, S.C., 1998. Seismic and hydrothermal evidence for a cracking event on the East Pacific Rise crest at 9°50'N. *Nature* 396, 159–161.
- Solomon, S.C., Huang, P.Y., Meinke, L., 1988. The seismic moment budget of slowly spreading ridges. *Nature* 346, 58–60.
- Sornette, A., Sornette, D., 1988. Self-organized criticality and earthquakes. *Europhys. Lett.* 9, 197–202.
- Spencer, S., Smith, D.K., Cann, J.R., Lin, J., McAllister, E., 1997. Structure and stability of non-transform discontinuities on the Mid-Atlantic Ridge between 24°N and 30°N. *Mar. Geophys. Res.* 19, 339–362.
- Sykes, L.R., 1970. Earthquake swarms and sea-floor spreading. *J. Geophys. Res.* 75, 6598–6611.
- Talandier, J., Okal, E.A., 1998. On the mechanism of conversion of seismic waves to and from T-wave in the vicinity of island shores. *Bull. Seismol. Soc. Am.* 88, 621–632.
- Teague, W.J., Carron, M.J., Hogan, P.J., 1990. A comparison between the generalized digital environmental model and levitus climatologies. *J. Geophys. Res.* 95, 7167–7183.
- Telesca, L., Cuomo, V., Lapenna, V., Macchiato, M., 2000a. Analysis of the time-scaling behaviour in the sequence of the aftershocks of the Bovec (Slovenia) April 12, 1998 earthquake. *Phys. Earth Planet. Inter.* 120, 315–326.
- Telesca, L., Cuomo, V., Lapenna, V., Vallianatos, F., 2000b. Self-similarity properties of seismicity in the southern Aegean area. *Tectonophysics* 321, 179–188.
- Telesca, L., Cuomo, V., Lapenna, V., Macchiato, M., 2001a. Identifying space-time clustering properties of the 1983–1997 Irpinia-Basilicata (southern Italy) seismicity. *Tectonophysics* 330, 93–102.
- Telesca, L., Cuomo, V., Lapenna, V., Macchiato, M., 2001b. Statistical analysis of fractal properties of point processes modeling seismic sequences. *Phys. Earth Planet. Inter.* 125, 65–83.
- Telesca, L., Cuomo, V., Lapenna, V., Macchiato, M., 2001c. Depth-dependent time-clustering behavior in seismicity of southern California. *Geophys. Res. Lett.* 22, 4323–4326.

- Telesca, L., Cuomo, V., Lapenna, V., Macchiato, M., 2002. On the methods to identify clustering properties in sequences of seismic time-occurrences. *J. Seismol.* 6, 125–134.
- Turner, S., Lowen, S.B., Feurstein, M.C., Heneghan, C., Feichtinger, H.G., Teich, M.C., 1997. Analysis, synthesis, and estimation of fractal-rate stochastic point process. *Fractals* 5, 565–596.
- Toomey, D.R., Solomon, S.C., Purdy, G.M., 1988. Microearthquakes beneath median valley of Mid-Atlantic Ridge near 23°N; tomography and tectonics. *J. Geophys. Res.* 93, 9093–9112.
- Turcotte, D.L., 1992. *Fractals and Chaos in Geology and Geophysics*. Cambridge University Press, Cambridge.
- Tolstoy, I., Ewing, W.M., 1950. The T phase of shallow-focus earthquakes. *Bull. Seismol. Soc. Am.* 40, 25–51.
- Walker, D.A., McCreery, C.S., Hiyoshi, Y., 1992. T-phase spectra, seismic moments, and tsunamigenesis. *Bull. Seismol. Soc. Am.* 82, 1275–1305.
- Wiemer, S., Wyss, M., 2000. Minimum magnitude of completeness in earthquake catalogs: examples from Alaska, the western United States, and Japan. *Bull. Seismol. Soc. Am.* 90, 859–869.
- Wilcock, W.S.D., Purdy, G.M., Solomon, S.C., 1990. Microearthquake evidence for extension across the Kane fracture zone. *J. Geophys. Res.* 95, 15,439–15,462.
- Wolfe, C.J., Purdy, G.M., Toomey, D.R., Solomon, S.C., 1995. Microearthquake characteristics and crustal velocity structure at 29° N on the Mid-Atlantic Ridge; the architecture of a slow spreading segment. *J. Geophys. Res.* 100, 24,449–24,472.
- Vinciguerra, S., Latora, V., Bicciato, S., Kamimura, R.T., 2001. Identifying and discriminating seismic patterns leading flank eruptions at Mt. Etna Volcano during 1981–1996. *J. Volcanol. Geotherm. Res.* 106, 211–228.